Soft-Clamped Silicon Nitride String Resonators at Millikelvin Temperatures

Thomas Gisler,[1] Mohamed Helal,[1] Deividas Sabonis,[1] Urs Grob,[1] Martin Héritier,[1] Christian L. Degen,[1] Amir H. Ghadimi,[2,*] and Alexander Eichler[1,†]

[1]*Laboratory for Solid State Physics, ETH Zürich, 8093 Zürich, Switzerland*

[2]*Centre Suisse d'Electronique et de Microtechnique SA (CSEM), 2002 Neuchâtel, Switzerland*

(Received 7 December 2021; accepted 3 August 2022; published 31 August 2022)

We demonstrate that soft-clamped silicon nitride strings with a large aspect ratio can be operated at mK temperatures. The quality factors (Q) of two measured devices show consistent dependency on the cryostat temperature, with soft-clamped mechanical modes reaching $Q > 10^9$ at roughly 46 mK. For low optical readout power, Q is found to saturate, indicating good thermalization between the sample and the stage it is mounted on. Our best device exhibits a calculated force sensitivity of 9.6 zN/$\sqrt{\text{Hz}}$ and a thermal decoherence time of 0.38 s, which bode well for future applications such as nanomechanical force sensing.

DOI: 10.1103/PhysRevLett.129.104301

Over the last few years, string and membrane micromechanical resonators made from high-stress silicon nitride (Si_3N_4) have established themselves as a powerful system for quantum engineering [1–7]. Applications range from electro-optomechanical transduction of quantum states [8,9] to scanning force microscopy [10], nuclear spin imaging [11,12], spin-phonon entanglement [13,14], and gravitational wave detection [15]. These applications profit immensely from cryogenic cooling of the resonator, both due to the lower thermomechanical noise and because the mechanical quality factor Q generally increases with reduced temperatures [16,17].

Even though Si_3N_4 resonators are expected to achieve their best performance at millikelvin temperatures, little is known about their actual properties (intrinsic Q, thermal conductivity, Young's modulus,...) under such conditions [16,18], in particular in the presence of optical absorption [15,17]. This is in part owed to the technical difficulties added by working in a dry dilution refrigerator, whose vibrations can furthermore add force and frequency noise [19]. More fundamental, however, is a concern that the interaction with an optical light field will induce heating in the mechanical device, making it difficult to consistently operate at mK temperatures. This issue could be strong for one-dimensional (string) devices [7,20,21], whose extreme aspect ratio is expected to lead to inefficient heat conduction.

In this work, we experimentally demonstrate that a corrugated soft-clamped Si_3N_4 string resonator with an aspect ratio of 200 000 (4 mm long, 20 nm thick) can be operated at temperatures as low as 46 ± 10 mK. We cool the strings in a dry dilution refrigerator with custom-built vibration isolation and a compact optical interferometer readout that allows us to characterize the resonator decay times during ringdown experiments. Through careful analysis, we infer that the string achieves thermal equilibrium with the sample plate for low optical readout power. Our best device reaches a mean value for the quality factor of $(2.3 \pm 0.12) \times 10^9$ at a resonance frequency of 1.406 MHz, corresponding to an intrinsic force sensitivity of 9.6 zN/$\sqrt{\text{Hz}}$ and a dissipation-limited coherence time of 0.38 s. Our work further shows a strong increase of Q at the lowest measured temperatures, providing fresh insight regarding the fundamental limitations of the coherence of the mechanical state.

We study soft-clamped nanostrings made from prestressed Si_3N_4 [6], see Fig. 1(a). The fabrication procedure is detailed in the Supplemental Material (SM). The devices are mounted in a Leiden CF450 dilution refrigerator with a mixing chamber base temperature of approximately $T_{\text{mc}} = 30$ mK, corresponding to a sample plate temperature as low as $T_{\text{plate}} = 40$ mK [22–24]. A spring suspension with soft copper braids between the mixing chamber and the sample stage reduces the in-coupling of mechanical noise. Two heaters at the sample stage allow for variations of the sample plate temperature between 46 and 194 mK.

Mechanical oscillations of the string are measured with a fiber-based optical interferometer, see Fig. 1(b) [23,25]. A piezoelectric actuator excites mechanical oscillations to the initial amplitude used for ringdown measurements. To reduce optical heating and backaction effects, we apply a stroboscopic measurement scheme [6] as shown in Fig. 1(c). A variable optical attenuator turns the illumination of the device on and off, enabling "ringdowns in the dark" whose progress is only intermittently probed. The photocurrent from the signal diode is amplified and measured with a lock-in detector. A phase-locked loop (PLL) is used to continuously adjust the local oscillator frequency of the lock-in amplifier to the mechanical resonance frequency during each "on" period.

 © 2022 American Physical Society

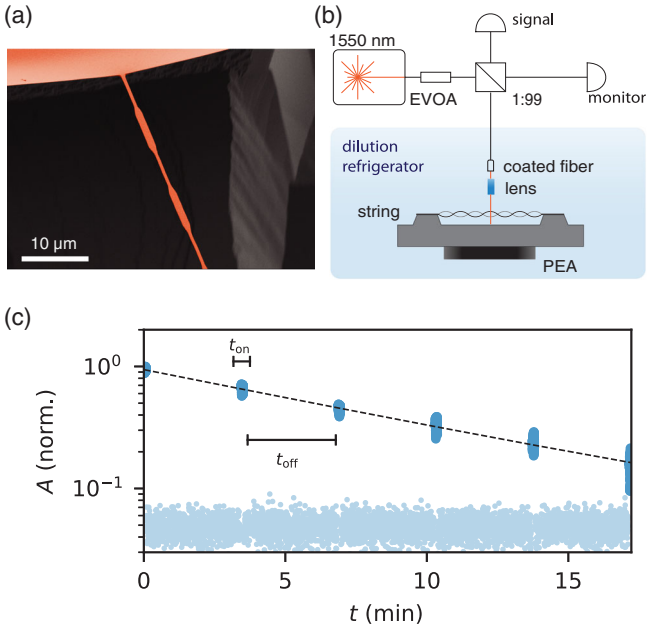

FIG. 1. Experimental setup and stroboscopic ringdown. (a) A false-colored SEM image of a string device similar to the ones used in this study. Shown is one clamping point and two unit cells. (b) Schematic illustration of the setup: A 1550 nm laser is used to measure the displacement of the Si_3N_4 beam. An electronic variable optical attenuator (EVOA) is used to switch on and off the optical readout for the stroboscopic measurements. The light reflected from the device interferes with the light reflected at the semitransparent coated fiber end. The light is focused with a gradient-index (GRIN) lens. The resonator motion is excited via a piezoelectric actuator (PEA) attached to the sample holder. The ac photodetector signal is recorded with a lock-in amplifier. (c) Stroboscopic ringdown measurement of the localized mode with frequency $f_0 = 1.406$ MHz at $T_{plate} = 46$ mK with $t_{on} = 5$ s and $t_{off} = 200$ s. The best fit for this particular ringdown yields $Q = 2.41 \pm 0.05 \times 10^9$ (95% confidence interval of the fit). Roughly 120 nW of laser power were focused on the resonator with a duty cycle of 0.02, yielding an average power of 2.4 nW.

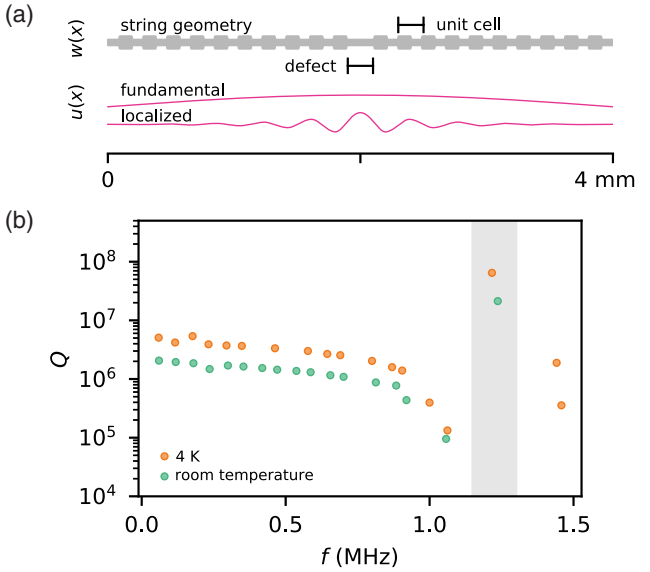

FIG. 2. String geometry and mode structure of device A. (a) Shape $w(x)$ of the 4 mm long corrugated beam with 10 unit cells on each side ($n = 10$) with a unit cell pitch of 100 μm, filling factor of 50% ($w_{min} = 500$ nm, $w_{max} = 1200$ nm), and a defect at the center with a width of 500 nm and length of 120 μm. The corresponding fundamental and localized mode shapes are shown as $u(x)$. (b) Quality factors of various mechanical modes of the corrugated string at room temperature (green) and at 4 K (orange). The string is 100 nm thick and grey shading indicates the extent of the phononic band gap.

Corrugated nanostrings exhibit a distinctive mode structure which is dictated by the number of unit cells and their geometry. The periodic corrugation creates a phononic crystal with a band gap [20]. This band gap spatially confines certain flexural modes, whose quality factors are enhanced due to a reduction in the clamping loss, see Fig. 2(a) [5,20,26]. For our initial study, we use a 4 mm-long and 100 nm-thick string, with a width varying between $w_{min} = 500$ nm and $w_{max} = 1200$ nm (Device A, see Table. I). For the particular string studied here, the soft-clamped mode has a resonance frequency of $f_{loc} = 1.237$ MHz at room temperature, well inside the phononic band gap indicated by a shaded region in Fig. 2(b). The effect of soft-clamping for the in–band-gap mode is clearly visible, since only this mode exceeds $Q > 10^7$.

Frequencies as well as quality factors of the mechanical modes are affected by changes in temperature. While the relative changes in frequency are small (e.g., $\delta f_{loc} = 20$ kHz for a localized mode with $f_{loc} = 1.237$ MHz), the quality factors increase significantly. In Fig. 2(b), we observe a consistent increase of the quality factors at 4 K compared to room temperature for all modes.

The stress, and therefore the dissipation dilution factor of prestressed resonators, increases for reduced beam cross sections [5,6]. In order to achieve higher quality factors, we repeat the measurements with two 20 nm-thick strings. We investigate strings with 12 unit cells, with DUC ratios of 1.1 (device B) and 1.2 (device C). The frequencies of the

TABLE I. List of devices. The temperature for the Q_{4K} is between 4 and 7 K. Defect-to-unit-cell (DUC) ratio is the ratio between the length of the defect and the pitch of a unit cell as indicated in Fig. 2(a).

	Device A	Device B	Device C
Length (mm)	4	4	4
Thickness (mm)	100	20	20
Unit cells	10	12	12
DUC ratio	1.2	1.1	1.2
f_{loc} (MHz)	1.237	1.443	1.406
$Q_{300K}(\times 10^6)$	21	73	100
$Q_{4K}(\times 10^6)$	65	540	730
$Q_{46\ mK}(\times 10^6)$		1600	2300

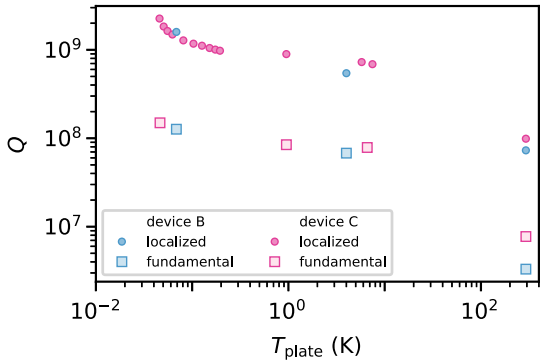

FIG. 3. Quality factor for various temperatures. Measured Q of two 20 nm-thick strings with $n = 12$ unit cells and different DUC ratio (device B: ratio 1.1, blue, device C: ratio 1.2, red) at various temperatures. For each string, circles and squares correspond to the localized and fundamental modes, respectively.

fundamental modes are $f_1^{B(C)} = 56.6$ kHz(56.3 kHz) and those of the localized mode (mode number 25) are $f_{\mathrm{loc}}^{B(C)} = 1.443$ MHz(1.406 MHz) at room temperature.

Figure 3 summarizes the Q values we measured for the fundamental and localized modes of the two devices B and C over the full temperature range. The localized modes show a constant and roughly tenfold higher quality factor compared to the fundamental modes, while the variations between the two devices are small. A reduction of the temperature from room temperature to 4 K leads to an improvement of all quality factor values by a factor ~10. Further cooling to the base temperature of the refrigerator ($T_{\mathrm{mc}} = 30$ mK) leads to another steep increase of Q for the localized mode of device C reaching up to $Q = 2 \times 10^9$. The heating experiment has exclusively been conducted with device C. A similar increase has been reported for metal-coated silicon strings [27] and with silicon nitride membrane resonators [15–18], but its microscopic origin remains unclear. To confirm the validity of our result, we performed careful studies as a function of average optical power and sample plate temperature that we present in the following. We note that the thermometer installed on the sample plate was not operational during these experiments. The temperature values reported here are the result of a careful calibration study between T_{plate} and T_{mc} that we performed in an additional cooldown. The calibration is shown in the SM [24].

The interaction of the string with the laser beam can induce two effects in the resonator modes: (i) on the one hand, optical absorption heats up the string above the lattice temperature of the stage it is mounted on. (ii) On the other hand, radiation pressure forces or photothermal forces act as positive or negative feedback that drive or damp a resonator mode [28,29]. To minimize these effects, we employ stroboscopic ringdown measurements, where light illuminates the string only for short periods t_{on} between "dark" periods t_{off} [see Fig. 1(c)]. The duty cycle D of a stroboscopic

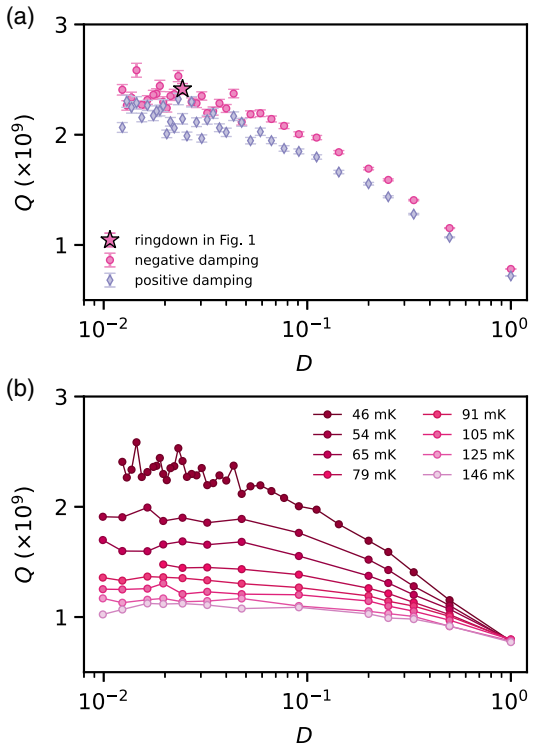

FIG. 4. Quality factor dependence on laser duty cycle and temperature. (a) Quality factor of device C as a function of the duty cycle D of the laser in the stroboscopic measurement. We kept $t_{\mathrm{on}} = 5$ s and varied t_{off}. Since the beam waist is larger than the string width, only around 120 nW of the 1.3 μW incident laser power is focused on the string while the laser is on. The interferometer is locked to values that induce either positive and negative damping (cf. SM [24]). Error bars correspond to 95% confidence interval of the best fit. (b) Q of device C for increasing sample plate sensor temperatures T_{plate}.

measurement is defined as $D = t_{\mathrm{on}}/(t_{\mathrm{on}} + t_{\mathrm{off}})$. We repeat ringdown measurements for positive and negative optical damping to characterize the influence of optomechanical feedback forces (cf. SM [24] for details regarding the fringe structure).

In Fig. 4(a), we see that the difference between opposite feedback forces is small. This indicates that the influence of radiation pressure or photothermal forces is minor. In contrast, the measured quality factor depends strongly on the duty cycle D, i.e., the average heating power arriving on the string surface. The effect is strongest when operating at the base temperature of the cryostat. The quality factor increases as we reduce D and plateaus for $D < 0.03$. This suggests that in this regime (i) either the string is well thermalized with the sample plate and the laser-induced heating is negligible, or (ii) Q becomes independent of temperature below $T_{\mathrm{plate}} \approx 200$ mK.

In Fig. 4(b), we show repeated measurements of Q as a function of D in the presence of a local heater mounted on the sample plate. Increasing T_{plate} leads to an immediate reduction of Q, demonstrating clearly that option (ii) is

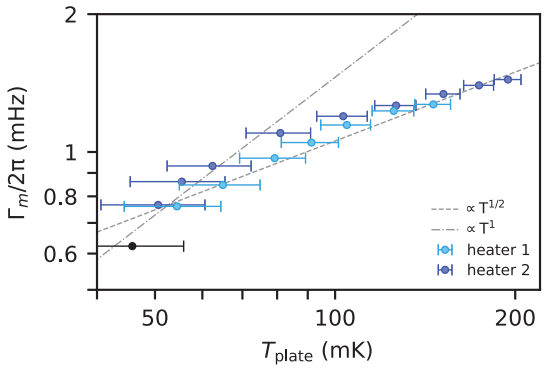

FIG. 5. Temperature-dependent dissipation coefficient. Γ_m measured as a function of T_{plate} with device C. Changes in T_{plate} were induced by two local heaters mounted on the sample stage (heater 1 and 2). The black dot corresponds to the case without heating. The dashed and dashed-dotted grey lines visualize the power laws $\Gamma_m \propto T^{\nu}$ with $\nu = 1/2$ [34] and $\nu = 1$ [30,31] predicted by the STM for one-dimensional resonators. Error bars indicate the calibration uncertainty of 10 mK of the sample stage thermometer.

wrong. We therefore conclude that option (i) is correct: our string resonators do thermalize with the sample plate temperature T_{plate}.

One possible explanation of the reduced dissipation below 200 mK is the nonresonant coupling between ensembles of defects in the material and the motion of the mechanical resonator [30]. The defects can be modeled as two-level systems (TLSs) in an asymmetric double-well potential [31,32]. The resonator oscillation induces localized strain variations that perturb the potential and couple the defects and phonons [33]. To compare our data to the standard tunneling model (STM), we plot $\Gamma_m = 2\pi f_{\mathrm{loc}}/Q$ as a function of T_{plate} in Fig. 5. Theoretical STM analyses on the role of TLSs for nanomechanical resonators predict a power law $\Gamma_m \propto T^{1/2}$ [34] or $\Gamma_m \propto T$ [30,31] for a quasi-one-dimensional string, with a plateau towards higher temperatures.

The comparison of experimental data to the STM has produced a variety of results in the past. With a range of different materials, measurements of quasi-one-dimensional devices were approximated as $\Gamma_m \propto T^{\nu}$ with $\nu = 1/3$ [35–37], $\nu = 2/3$ [38], or $\nu = 1$ [27,30]. A saturation of Γ_m towards low temperatures was accounted for by the form $\Gamma_m \propto [1 + (T/T_0)^{\nu}]$, with the free parameters $T_0 = 0.3$ K and $\nu = 1.6$ [22,34]. Our data show a plateau of the dissipation above $T_{\mathrm{plate}} \approx 150$ mK but no saturation at the lower end of the accessible temperature range.

The implications of our measurements remain to be investigated. In future work, we will study the possible presence of surface adsorbates that can introduce additional damping [39], and their partial desorption with strong local heaters [40].

Looking forward, high Q and low device temperatures are essential when using mechanical resonators for the detection of small forces. The nanostrings investigated in this work have a thermal noise-limited, single-sided force sensitivity estimated as [41]

$$\sqrt{S_f} = \sqrt{4k_B T_{\mathrm{plate}} m_{\mathrm{eff}} \Gamma_m} = 9.6\ \mathrm{zN}/\sqrt{\mathrm{Hz}} \qquad (1)$$

where k_B is the Boltzmann constant, $T_{\mathrm{plate}} = 46$ mK is the device temperature, $\Gamma_m = 2\pi f_0/Q$ is the dissipation coefficient for a resonance frequency f_0, and the effective mass $m_{\mathrm{eff}} = 9.3$ pg is extracted from numerically solving the one-dimensional Euler-Bernoulli equation [26]. Our best device therefore attains a force sensitivity similar to that of a single carbon nanotube [42,43], in spite of the roughly 10^6 times larger mass. In contrast to carbon nanotubes with a diameter of ≈1 nm, our top-down patterned Si_3N_4 strings are large enough to envisage mounting a molecular sample on them. This provides an interesting perspective for ultrasensitive force detection experiments, for instance in the context of nanoscale magnetic resonance imaging [12,44–46]. A side-by-side comparison with the performance of a state-of-the-art cantilever sensor confirms this assessment (cf. SM [24]).

Low temperatures and high quality factors are also important for increasing the quantum coherence time of the resonator's oscillation states [18,47]. Dissipation imposes a limit to the coherence time, yielding in our case

$$\gamma_{\mathrm{diss}}^{-1} \approx \frac{1}{n\Gamma_m} = \frac{Q\hbar}{k_B T_{\mathrm{plate}}} = 0.38\ \mathrm{s} \qquad (2)$$

where $n \approx 1000$ is the phonon occupation number of the resonator mode and $\hbar$ is the reduced Planck constant. We emphasize, however, that frequency fluctuations [48] can significantly reduce this coherence time in practice. The characterization of frequency fluctuations in these corrugated string devices is an important topic to be explored in future studies.

A second crucial objective is to reduce the detection noise when reading out the nanomechanical oscillation. The simple interferometer used in the current setup is not optimized for string devices and produces significant additional readout noise, making the detection of thermomechanical force noise impossible. Integrated optomechanical readout [49,50] can mitigate this problem. Increasing the vacuum optomechanical coupling rate g_0 [28] will allow better detection sensitivity for the same added heating. This is possible because the optomechanical cooperativity scales as G^2, while absorption of light, in a rough approximation, is estimated to increases only linearly with G [51,52].

In summary, we cooled and operated a Si_3N_4 string to a bath temperature of 46 mK, where it achieved a force sensitivity of $9.6\ \mathrm{zN}/\sqrt{\mathrm{Hz}}$ and a dissipation-limited

coherence time of 0.38 s. We measure mechanical Q as high as 2.3×10^9, more than 20× improvement compared to room temperature. We observe a sudden increase of Q at the lowest temperatures of our dilution refrigerator, implying that further improvements should be achieved with a larger cooling power at base temperature and with better thermalization of the sample plate. The microscopic origin of the damping and decoherence in our devices is not fully understood. However, the isolated nature of these localized modes provides an unique avenue for further work. Because of their simple geometry and strong isolation from environmental influences, nanomechanical strings offer an ideal system to test model predictions.

This work was supported by the Swiss National Science Foundation (CRSII5_177198/1) and an ETH Zurich Research Grant (ETH-51 19-2).

*Corresponding author.
amir.ghadimi@csem.ch
†Corresponding author.
eichlera@ethz.ch

[1] S. S. Verbridge, H. G. Craighead, and J. M. Parpia, A megahertz nanomechanical resonator with room temperature quality factor over a million, Appl. Phys. Lett. **92**, 013112 (2008).

[2] G. Anetsberger, E. Gavartin, O. Arcizet, Q. P. Unterreithmeier, E. M. Weig, M. L. Gorodetsky, J. P. Kotthaus, and T. J. Kippenberg, Measuring nanomechanical motion with an imprecision below the standard quantum limit, Phys. Rev. A **82**, 061804(R) (2010).

[3] C. Reetz, R. Fischer, G. G. T. Assumpção, D. P. McNally, P. S. Burns, J. C. Sankey, and C. A. Regal, Analysis of Membrane Phononic Crystals with Wide Band Gaps and Low-Mass Defects, Phys. Rev. Applied **12**, 044027 (2019).

[4] C. Reinhardt, T. Müller, A. Bourassa, and J. C. Sankey, Ultralow-Noise SiN Trampoline Resonators for Sensing and Optomechanics, Phys. Rev. X **6**, 021001 (2016).

[5] Y. Tsaturyan, A. Barg, E. S. Polzik, and A. Schliesser, Ultracoherent nanomechanical resonators via soft clamping and dissipation dilution, Nat. Nanotechnol. **12**, 776 (2017).

[6] A. H. Ghadimi, S. A. Fedorov, N. J. Engelsen, M. J. Bereyhi, R. Schilling, D. J. Wilson, and T. J. Kippenberg, Elastic strain engineering for ultralow mechanical dissipation, Science **360**, 764 (2018).

[7] A. Beccari, M. J. Bereyhi, R. Groth, S. A. Fedorov, A. Arabmoheghi, N. J. Engelsen, and T. J. Kippenberg, Hierarchical tensile structures with ultralow mechanical dissipation, Nat. Commun. **13**, 3097 (2022).

[8] T. Bagci, A. Simonsen, S. Schmid, L. G. Villanueva, E. Zeuthen, J. Appel, J. M. Taylor, A. Sørensen, K. Usami, A. Schliesser, and E. S. Polzik, Optical detection of radio waves through a nanomechanical transducer, Nature (London) **507**, 81 (2014).

[9] R. W. Andrews, R. W. Peterson, T. P. Purdy, K. Cicak, R. W. Simmonds, C. A. Regal, and K. W. Lehnert, Bidirectional and efficient conversion between microwave and optical light, Nat. Phys. **10**, 321 (2014).

[10] D. Hälg, T. Gisler, Y. Tsaturyan, L. Catalini, U. Grob, M.-D. Krass, M. Héritier, H. Mattiat, A.-K. Thamm, R. Schirhagl, E. C. Langman, A. Schliesser, C. L. Degen, and A. Eichler, Membrane-Based Scanning Force Microscopy, Phys. Rev. Applied **15**, L021001 (2021).

[11] R. Fischer, D. P. McNally, C. Reetz, G. G. T. Assumpção, T. Knief, Y. Lin, and C. A. Regal, Spin detection with a micromechanical trampoline: Towards magnetic resonance microscopy harnessing cavity optomechanics, New J. Phys. **21**, 043049 (2019).

[12] J. Košata, O. Zilberberg, C. L. Degen, R. Chitra, and A. Eichler, Spin Detection via Parametric Frequency Conversion in a Membrane Resonator, Phys. Rev. Applied **14**, 014042 (2020).

[13] T. M. Karg, B. Gouraud, C. T. Ngai, G.-L. Schmid, K. Hammerer, and P. Treutlein, Light-mediated strong coupling between a mechanical oscillator and atomic spins 1 meter apart, Science **369**, 174 (2020).

[14] R. A. Thomas, M. Parniak, C. Østfeldt, C. B. Møller, C. Bærentsen, Y. Tsaturyan, A. Schliesser, J. Appel, E. Zeuthen, and E. S. Polzik, Entanglement between distant macroscopic mechanical and spin systems, Nat. Phys. **17**, 228 (2021).

[15] M. A. Page, M. Goryachev, H. Miao, Y. Chen, Y. Ma, D. Mason, M. Rossi, C. D. Blair, L. Ju, D. G. Blair, A. Schliesser, M. E. Tobar, and C. Zhao, Gravitational wave detectors with broadband high frequency sensitivity, Commun. Phys. **4**, 27 (2021).

[16] M. Yuan, M. A. Cohen, and G. A. Steele, Silicon nitride membrane resonators at millikelvin temperatures with quality factors exceeding 10^8, Appl. Phys. Lett. **107**, 263501 (2015).

[17] R. Fischer, N. Kampel, G. Assumpção, P.-L. Yu, K. Cicak, R. Peterson, R. Simmonds, and C. Regal, Optical probing of mechanical loss of a Si_{3}N_{4} membrane below 100 mK, arXiv:1611.00878.

[18] Y. Seis, T. Capelle, E. Langman, S. Saarinen, E. Planz, and A. Schliesser, Ground state cooling of an ultracoherent electromechanical system, Nat. Commun. **13**, 1507 (2022).

[19] R. Kalra, A. Laucht, J. P. Dehollain, D. Bar, S. Freer, S. Simmons, J. T. Muhonen, and A. Morello, Vibration-induced electrical noise in a cryogen-free dilution refrigerator: Characterization, mitigation, and impact on qubit coherence, Rev. Sci. Instrum. **87**, 073905 (2016).

[20] A. H. Ghadimi, D. J. Wilson, and T. J. Kippenberg, Radiation and internal loss engineering of high-stress silicon nitride nanobeams, Nano Lett. **17**, 3501 (2017).

[21] A. Beccari, D. A. Visani, S. A. Fedorov, M. J. Bereyhi, V. Boureau, N. J. Engelsen, and T. J. Kippenberg, Strained crystalline nanomechanical resonators with quality factors above 10 billion, Nat. Phys. **18**, 436 (2022).

[22] Y. Tao, J. M. Boss, B. A. Moores, and C. L. Degen, Single-crystal diamond nanomechanical resonators with quality factors exceeding one million, Nat. Commun. **5**, 3638 (2014).

[23] M. Héritier, A. Eichler, Y. Pan, U. Grob, I. Shorubalko, M. D. Krass, Y. Tao, and C. L. Degen, Nanoladder

cantilevers made from diamond and silicon, Nano Lett. **18**, 1814 (2018).
[24] See Supplemental Material at http://link.aps.org/supplemental/10.1103/PhysRevLett.129.104301 for additional setup descriptions, more measurement data.
[25] D. Rugar and P. Grütter, Mechanical Parametric Amplification and Thermomechanical Noise Squeezing, Phys. Rev. Lett. **67**, 699 (1991).
[26] S. A. Fedorov, N. J. Engelsen, A. H. Ghadimi, M. J. Bereyhi, R. Schilling, D. J. Wilson, and T. J. Kippenberg, Generalized dissipation dilution in strained mechanical resonators, Phys. Rev. B **99**, 054107 (2019).
[27] O. Maillet, D. Cattiaux, X. Zhou, R. R. Gazizulin, O. Bourgeois, A. D. Fefferman, and E. Collin, Nanomechanical damping via electron-assisted relaxation of two-level systems, arXiv:2009.03804.
[28] M. Aspelmeyer, T. J. Kippenberg, and F. Marquardt, Cavity optomechanics, Rev. Mod. Phys. **86**, 1391 (2014).
[29] C. H. Metzger and K. Karrai, Cavity cooling of a microlever, Nature (London) **432**, 1002 (2004).
[30] B. D. Hauer, P. H. Kim, C. Doolin, F. Souris, and J. P. Davis, Two-level system damping in a quasi-one-dimensional optomechanical resonator, Phys. Rev. B **98**, 214303 (2018).
[31] R. O. Behunin, F. Intravaia, and P. T. Rakich, Dimensional transformation of defect-induced noise, dissipation, and nonlinearity, Phys. Rev. B **93**, 224110 (2016).
[32] W. A. Phillips, Two-level states in glasses, Rep. Prog. Phys. **50**, 1657 (1987).
[33] G. J. Grabovskij, T. Peichl, J. Lisenfeld, G. Weiss, and A. V. Ustinov, Strain tuning of individual atomic tunneling systems detected by a superconducting qubit, Science **338**, 232 (2012).
[34] C. Seoánez, F. Guinea, and A. H. Castro Neto, Surface dissipation in nanoelectromechanical systems: Unified description with the standard tunneling model and effects of metallic electrodes, Phys. Rev. B **77**, 125107 (2008).
[35] G. Zolfagharkhani, A. Gaidarzhy, S.-B. Shim, R. L. Badzey, and P. Mohanty, Quantum friction in nanomechanical oscillators at millikelvin temperatures, Phys. Rev. B **72**, 224101 (2005).
[36] S. B. Shim, J. S. Chun, S. W. Kang, S. W. Cho, S. W. Cho, Y. D. Park, P. Mohanty, N. Kim, and J. Kim, Micromechanical resonators fabricated from lattice-matched and etch-selective GaAs/InGaP/GaAs heterostructures, Appl. Phys. Lett. **91**, 133505 (2007).
[37] M. Imboden and P. Mohanty, Evidence of universality in the dynamical response of micromechanical diamond resonators at millikelvin temperatures, Phys. Rev. B **79**, 125424 (2009).
[38] K. J. Lulla, M. Defoort, C. Blanc, O. Bourgeois, and E. Collin, Evidence for the Role of Normal-State Electrons in Nanoelectromechanical Damping Mechanisms at Very Low Temperatures, Phys. Rev. Lett. **110**, 177206 (2013).
[39] M. Héritier, R. Pachlatko, Y. Tao, J. M. Abendroth, C. L. Degen, and A. Eichler, Spatial Correlation between Fluctuating and Static Fields Over Metal and Dielectric Substrates, Phys. Rev. Lett. **127**, 216101 (2021).
[40] D. Martinez-Martin, R. Longuinhos, J. G. Izquierdo, A. Marele, S. S. Alexandre, M. Jaafar, J. M. Gómez-Rodríguez, L. Bañares, J. M. Soler, and J. Gomez-Herrero, Atmospheric contaminants on graphitic surfaces, Carbon **61**, 33 (2013).
[41] P. R. Saulson, Thermal noise in mechanical experiments, Phys. Rev. D **42**, 2437 (1990).
[42] J. Moser, J. Güttinger, A. Eichler, M. J. Esplandiu, D. E. Liu, M. I. Dykman, and A. Bachtold, Ultrasensitive force detection with a nanotube mechanical resonator, Nat. Nanotechnol. **8**, 493 (2013).
[43] S. L. de Bonis, C. Urgell, W. Yang, C. Samanta, A. Noury, J. Vergara-Cruz, Q. Dong, Y. Jin, and A. Bachtold, Ultrasensitive displacement noise measurement of carbon nanotube mechanical resonators, Nano Lett. **18**, 5324 (2018).
[44] M. Poggio and C. L. Degen, Force-detected nuclear magnetic resonance: Recent advances and future challenges, Nanotechnology **21**, 342001 (2010).
[45] J. M. Nichol, T. R. Naibert, E. R. Hemesath, L. J. Lauhon, and R. Budakian, Nanoscale Fourier-Transform Magnetic Resonance Imaging, Phys. Rev. X **3**, 031016 (2013).
[46] U. Grob, M.-D. Krass, M. Héritier, R. Pachlatko, J. Rhensius, J. Košata, B. A. J. Moores, H. Takahashi, A. Eichler, and C. L. Degen, Magnetic resonance force microscopy with a one-dimensional resolution of 0.9 nanometers, Nano Lett. **19**, 7935 (2019).
[47] M. Rossi, D. Mason, J. Chen, Y. Tsaturyan, and A. Schliesser, Measurement-based quantum control of mechanical motion, Nature (London) **563**, 53 (2018).
[48] K. Y. Fong, W. H. P. Pernice, and H. X. Tang, Frequency and phase noise of ultrahigh Q silicon nitride nanomechanical resonators, Phys. Rev. B **85**, 161410(R) (2012).
[49] R. Schilling, H. Schütz, A. H. Ghadimi, V. Sudhir, D. J. Wilson, and T. J. Kippenberg, Near-Field Integration of a SiN Nanobeam and a SiO_2 Microcavity for Heisenberg-Limited Displacement Sensing, Phys. Rev. Applied **5**, 054019 (2016).
[50] J. Guo, R. Norte, and S. Gröblacher, Feedback Cooling of a Room Temperature Mechanical Oscillator Close to its Motional Ground State, Phys. Rev. Lett. **123**, 223602 (2019).
[51] D. J. Wilson, V. Sudhir, N. Piro, R. Schilling, A. Ghadimi, and T. J. Kippenberg, Measurement-based control of a mechanical oscillator at its thermal decoherence rate, Nature (London) **524**, 325 (2015).
[52] A. H. Ghadimi, Ultra-coherent nano-mechanical resonators for quantum optomechanics at room temperature, Technical Report, EPFL, 2018, 10.5075/epfl-thesis-8967.